Dimuon production by neutrinos in the Fermilab 15-ft bubble chamber at the Tevatron

V. Jain,[g,*] F. A. Harris,[g] M. Aderholz,[l] M. M. Aggarwal,[e] H. Akbari,[q,†] P. P. Allport,[k,‡]
P. V. K. S. Baba,[j] S. K. Badyal,[j] M. Barth,[c] J. P. Baton,[o] H. H. Bingham,[a]
E. B. Brucker,[p] R. A. Burnstein,[i] J. R. Campbell,[h] R. J. Cence,[g] T. K. Chatterjee,[e]
E. F. Clayton,[h] G. Corrigan,[k] C. Coutures,[o] D. Deprospo,[n] Devanand,[j] E. De Wolf,[c,§]
P. J. W. Faulkner,[b] W. B. Fretter,[a] V. K. Gupta,[j] J. Guy,[m] J. Hanlon,[f] G. G. Harigel,[d]
M. A. Jabiol,[o] P. Jacques,[n] G. T. Jones,[b] M. D. Jones,[g] T. Kafka,[q] M. Kalelkar,[n]
P. Kasper,[o,**] G. L. Kaul,[j] M. Kaur,[e] J. M. Kohli,[e] E. L. Koller,[p] R. J. Krawiec,[b]
M. Lauko,[n] J. Lys,[a] P. Marage,[c] R. H. Milburn,[q] D. B. Miller,[h] I. S. Mittra,[e]
M. M. Mobayyen,[h] J. Moreels,[c] D. R. O. Morrison,[d] G. Myatt,[k] P. Nailor,[h] R. Naon,[i]
A. Napier,[q] M. Neveu,[o] D. Passmore,[q] M. W. Peters,[g] V. Z. Peterson,[g] R. Plano,[n]
N. K. Rao,[j] H. A. Rubin,[i] J. Sacton,[c] B. Saitta,[q,††] P. Schmid,[d] N. Schmitz,[l]
J. Schneps,[q] R. Sekulin,[m] S. Sewell,[m] J. B. Singh,[e] P. M. Sood,[e] W. Smart,[f]
P. Stamer,[n,‡‡] K. E. Varvell,[b] W. Venus,[m] L. Verluyten,[c,§] L. Voyvodic,[f] H. Wachsmuth,[d]
S. Wainstein,[h] S. Willocq,[c,§§] and G. P. Yost[a]

[a]University of California, Berkeley, California 94720
[b]University of Birmingham, B15 2TT, United Kingdom
[c]Inter-University Institute for High Energies, Université Libre de Bruxelles, Vrije,
Universiteit te Brussels, B-1050 Brussels, Belgium
[d]CERN, CH-1211 Geneva 23, Switzerland
[e]Panjab University, Chandigarh 160014, India
[f]Fermilab, P.O. Box 500, Batavia, Illinois 60510
[g]University of Hawaii, Honolulu, Hawaii 96822
[h]Imperial College of Science and Technology, London, SW7 2AZ, United Kingdom
[i]Illinois Institute of Technology, Chicago, Illinois 60616
[j]University of Jammu, Jammu 180001, India
[k]Department of Nuclear Physics, Oxford, OX1 3RH, United Kingdom
[l]Max-Planck-Institut fuer Physik und Astrophysik, D-800 Muenchen 40, Federal Republic of Germany
[m]Rutherford Appleton Laboratory, Chilton, Didcot, OX11 0QX, United Kingdom
[n]Rutgers University, New Brunswick, New Jersey 08903
[o]Département de Physique des Particules Élémentaires, Centre d'Etudes Nucleaires,
Saclay, F-91191 Gif-sur-Yvette, France
[p]Stevens Institute of Technology, Hoboken, New Jersey 07030
[q]Tufts University, Medford, Massachusetts 02155
(Received 27 September 1989)

The Fermilab 15-ft bubble chamber has been exposed to a quadrupole triplet neutrino beam produced at the Tevatron. The ratio of ν to $\bar{\nu}$ in the beam is approximately 2.5. The mean event energy for ν-induced charged-current events is 150 GeV, and for $\bar{\nu}$-induced charged-current events it is 110 GeV. A total of 64 dimuon candidates (1 $\mu^+\mu^+$, 52 $\mu^-\mu^+$ and $\mu^+\mu^-$, and 11 $\mu^-\mu^-$) is observed in the data sample of approximately 13 300 charged-current events. The number and properties of the $\mu^-\mu^-$ and $\mu^+\mu^+$ candidates are consistent with their being produced by background processes, the important sources being π and K decay and punchthrough. The 90%-C.L. upper limit for $\mu^-\mu^-/\mu^-$ for muon momenta above 4 GeV/c is 1.2×10^{-3}, and for momenta above 9 GeV/c this limit is 1.1×10^{-3}. The opposite-sign-dimuon–to–single-muon ratio is $(0.62\pm0.13)\%$ for muon momenta above 4 GeV/c. There are eight neutral strange particles in the opposite-sign sample, leading to a rate per dimuon event of 0.65 ± 0.29. The opposite-sign-dimuon sample is consistent with the hypothesis of charm production and decay.

I. INTRODUCTION

The Fermilab 15-ft bubble chamber was exposed to a high-energy neutrino beam at the Tevatron (experiment E632) and data were collected during two separate runs. The neutrino energy spectrum extended to greater than 600 GeV, and approximately one-third of the neutrino interactions were at energies above 200 GeV. A big bubble chamber is a well-understood and reasonably unbiased detector and thus well suited to a search for new phenomena, which is the primary aim of the present experiment. Multilepton events may indicate the presence of new particles, and in this paper we report results on ν- and $\bar{\nu}$-induced dimuon events in the data collected during the first run.

Opposite-sign-dilepton [$\mu\mu$ (Refs. 1–9) and μe (Refs.

9-20)] events have been observed in the past and their characteristics are explained by single-charm production and subsequent semileptonic decay. The observed rates are 0.5% to 1% of the charged-current rate.

The like-sign-dilepton rate is controversial. Some experiments[7,21-27] have reported signals that were several times the rate expected within the standard model, where the dominant contribution is from charm pair production. Other experiments have found rates or upper limits that were consistent with the standard model.[4,6,9,16,17,20,28,29] The reported rates are generally less than 10^{-3} of the charged-current rate. The expected standard-model rate[30-33] increases with energy and is around 10^{-5} at 200 GeV. A major problem is the evaluation of background contributions. Leptons from decays of long-lived particles (predominantly π's and K's) are considered as background (or nonprompt), whereas those from decays of short-lived particles (e.g., charm and bottom) are considered as part of the signal (or prompt). Generally, counter experiments have estimated this background with Monte Carlo programs, and the input to these programs is data, taken from bubble-chamber experiments, on hadrons produced in neutrino interactions. Independent of rate, with the attendant background uncertainty, at least one experiment[34] found evidence (at the $2-3\sigma$ level) of a difference in kinematic properties between the observed like-sign dimuon candidates and the "background" events.

Some like-sign-dilepton results[7,24] suggested a rapid increase at high energy, $E_\nu \geq 200$ GeV (this energy region can be explored in the present experiment, E632). A recent counter experiment[29] at the Tevatron has reported no such rapid increase and finds a rate consistent with the standard-model predictions. Clearly, it is important to check this latter result. Compared to that experiment, the present experiment has the advantage that it measures, in the same apparatus and at the same energy, the hadron production that is the source of the all-important background (Ref. 29 had to extrapolate hadron rates from lower-energy experiments). In addition, the present experiment detects muons with momenta down to 4 GeV/c, and candidates can be examined in greater detail. However, the present experiment has the disadvantage of low statistics.

We describe the apparatus, the event-selection criteria, and the backgrounds in Secs. II, III, and IV, respectively. In Sec. V we describe the method used to account for the missing hadronic energy, in both the dimuon and single-muon event samples. In Sec. VI we present the detection efficiency of dimuon events and calculate event rates. In Sec. VII we compare the opposite-sign-dimuon sample with the predictions of a charm Monte Carlo simulation (and background predictions), and in Sec. VIII we present distributions comparing the like-sign sample with background predictions. Section IX contains a summary of our results.

II. APPARATUS

The neutrino beam was formed using 800-GeV protons from the Tevatron and the quadrupole triplet train, tuned to 300 GeV/c. The target was a water-cooled beryllium oxide cylinder. Each beam spill was typically 2-3 ms long. The ratio[35,36] of ν's to $\bar{\nu}$'s in the beam is approximately 2.5, producing a ν to $\bar{\nu}$ event ratio of 5.1. The ν and $\bar{\nu}$ beams have mean energies of 90 and 75 GeV, whereas the mean energies of ν- and $\bar{\nu}$-induced charged-current (CC) events are 150 and 110 GeV, respectively. The calculated energy spectra[35,36] of the CC events are shown in Fig. 1.

The 15-ft bubble chamber (liquid volume ~ 30 m^3) was filled with a 75%-25% molar neon-hydrogen mixture. The radiation length, interaction length, and density for the mixture was 40 cm, 153 cm, and 0.70 g/cm^3, respectively. A 3-T magnetic field inside the chamber was used to determine the momentum of the charged particles. The bubble chamber was equipped with three conventional cameras and one high-resolution conventional camera. In addition, this run was also an engineering run for high-resolution holographic optics in a big bubble chamber. The general features of the bubble chamber are shown in Fig. 2.

The bubble chamber was equipped with a new external muon identifier (EMI) and internal picket fence (IPF). Both the EMI and the IPF (Ref. 37) were constructed out of proportional drift tubes and were arranged as shown in Fig. 3. The EMI was used for muon identification, whereas the IPF aided in determining the time of the event. The IPF, which covered 290° in azimuth, surrounded the inner tank of the bubble chamber and was attached to the bubble-chamber magnet. The IPF half on the upstream end of the bubble chamber was labeled IPFA, whereas the half on the downstream end of the chamber was labeled IPFB. Each IPF half consisted of 48 cans, each can being 220 cm long, 11.0 cm wide, and 2.2 cm thick. The area covered by the IPF was 23.2 m^2. The cans were symmetrically arranged with respect to the midplane of the bubble chamber. A single can contained 24 stainless-steel tubes arranged in two layers, each tube being 220 cm long and containing a 50-μm-diameter gold-plated tungsten wire. The wires in each can were grouped together to form four signals, two in each layer. The two layers were staggered with respect to each other, by half a tube width, to increase geometric and electronic efficiency.
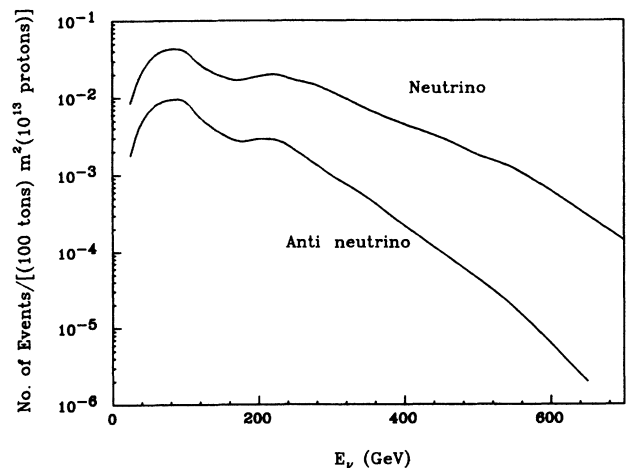

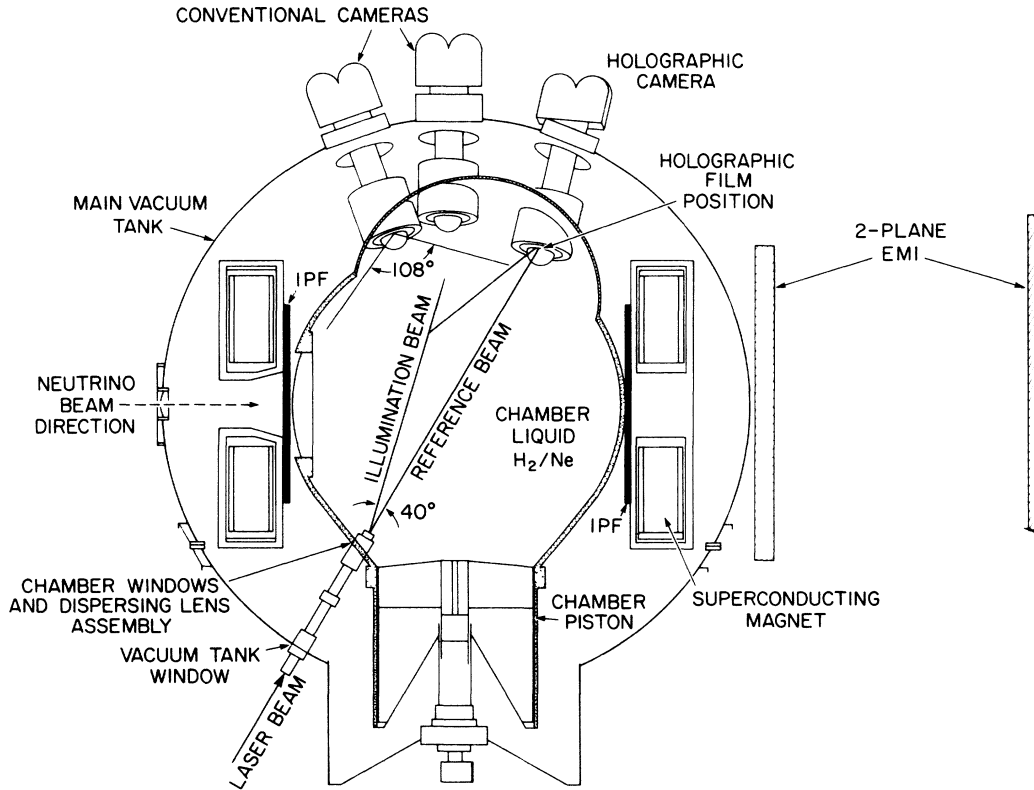FIG. 1. Calculated energy spectra of charged-current events.

FIG. 2. Side view of the 15-ft bubble chamber.

The EMI consisted of three planes placed outside the bubble-chamber vacuum tank. The first plane directly downstream of the bubble chamber, EMIB, was separated from the chamber by 3–5 hadronic interaction lengths (chamber vessel, magnet coils, support structure, and zinc). The second downstream plane, EMIC, was behind another 4–6 interaction lengths (lead and concrete shielding blocks). The small plane, EMIA, to the right

FIG. 3. Top view of the EMI/IPF. Not to scale.

side of the bubble chamber is not used in the present analysis. The EMI consisted of proportional drift tubes formed out of aluminum extrusions, with each extrusion containing two layers of drift tubes. The tubes were 22.2 mm on the side (inside dimension), and had a wall thickness of 3.18 mm. The two layers were staggered by half a tube, with respect to each other, to increase geometric and electronic efficiency. The extrusions are fastened together to form a plane. Each of the two EMI planes used in this analysis covered an area of 24.3 m^2, whereas EMIA had an area of 8.8 m^2. EMIB was composed of six layers of wires and measured coordinates along the horizontal and vertical axes (H and V) and an axis which was 36.5° to the vertical (U), whereas EMIA and EMIC had only four layers of wires and measured coordinates along the horizontal and vertical axes (H and V).
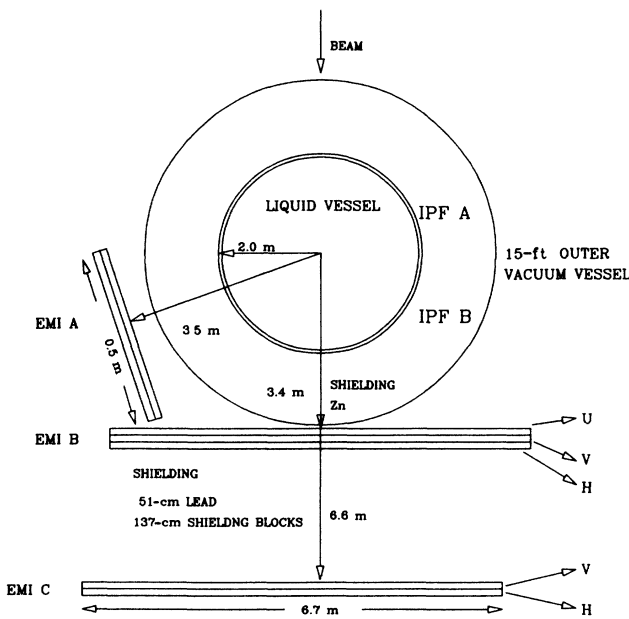
Signals from both the EMI and the IPF were amplified and discriminated at the detector. Signals from fifteen EMI or twelve IPF tubes were multiplexed onto one cable and sent to the control room, where they were demultiplexed and read via CAMAC. The data were divided into 1-μs time intervals. Hits from one time interval could spill over into the next one, and hence in this analysis two adjacent time intervals are combined, if both contain hits, to form one time slot. A time slot is then either 1 or 2 μs wide.

In the first run we collected 155 000 conventional photographs, corresponding to 2.5×10^{17} protons on target. In the present analysis, we use data corresponding to 2.25×10^{17} protons on target which correspond to 13 300 CC events in the fiducial volume of 15 m^3.

III. EVENT SELECTION

The EMI/IPF system is used in a novel way to find multimuon candidates.[38] We select such events by using the measured event vertices in conjunction with the EMI and IPF data. First, the film is scanned for neutrino events and the vertex of each event found is measured. Tracks are then constructed by joining the event vertices to time-coincident hits in the EMI planes, taking the magnetic field into account. This procedure is done separately in the horizontal and vertical views, and the U coordinate in the EMIB plane is used to remove accidental combinations of (H, V) hits. Cuts are imposed on the direction and radius of curvature (thus indirectly on the momentum) of these tracks, and on their match with hits in IPFB. These cuts are determined using a sample of measured tracks and are designed to have a very high efficiency for accepting real muons with momentum greater than 4 GeV/c.

Only those events which have at least two muon candidate tracks in both the H and V planes are selected at this stage (20% of all events in the fiducial volume). They are then examined at the scan table to ensure that they indeed have at least two charged particles which leave the bubble chamber without visibly interacting (called leaving tracks), and that each of these particles has a momentum greater than 3 GeV/c (to have a high efficiency for keeping muons above 4 GeV/c). Events are also required to be within a restricted fiducial volume (15 m^3). Using this technique only 9% of all events in the entire data sample are selected as possible dimuon candidates.

After event measurement and geometric reconstruction, leaving tracks are extrapolated through the absorber and the magnetic field to the IPF and EMI. The predicted positions are compared with the hit tubes in the EMI and a two-plane confidence level is calculated. Tracks are required to match with hits in the H and V views in both EMIB and EMIC in the same time slot. Tracks which have a confidence level greater than 1% are labeled muons. We require the muon momenta to be greater than 4 GeV/c. To reduce the contamination due to background events we impose additional cuts: requiring a match in the U coordinate in the first EMI plane, activity in the downstream IPF during the event time slot (either each muon has a match or there are at least 2 "bunches"[39] in the event time slot), and requiring that the muon candidates have separate hits along the H and V coordinates of EMIC.

Using these selection criteria, we identify 52 opposite-sign- and 12 like-sign-dimuon candidates. From a small sample (14% of the entire data sample) of events where only the leaving tracks are measured, we estimate that after correcting for inefficiencies (see below) there are $11\,130\pm320$ v-induced and $2\,170\pm150$ $\bar{v}$-induced charged-current events with muon momentum greater than 4 GeV/c in the total sample. All the dimuon candidates were completely measured, i.e., all primary tracks and all γ's, neutral interactions (N^*'s), and neutral strange particles (V^0's) associated with the primary vertex are measured. Also, 500 v-induced and 100 $\bar{v}$-induced

CC events were measured for comparison with the dimuon sample. The CC sample is not measured as completely as the dimuon sample, the difference being that only the five highest energy γ's and the high-energy N^*'s are measured in the CC sample.

IV. BACKGROUNDS

The 64 dimuon candidates contain background due to charged-current events where either a hadron undergoes nonprompt muon decay, which is not detected, or a hadron leaving the bubble chamber without interacting is mislabeled as a muon by the EMI, thus producing a fake dimuon event.

A. Decay background

This background is due to π's and K's that are produced in charged-current events. Because the interaction length in the bubble-chamber liquid is comparable to the chamber radius, some π's and K's decay, into a μ and a v (or $\bar{v}$), before interacting. For π's and K's with momenta above 4 GeV/c, the decay muon may follow the direction of the parent particle closely enough that it hits the EMI near the parent's predicted position, and in many instances, the EMI match can pass the 1% cut on the two-plane confidence level, thereby producing a fake primary muon. The major fraction of this background is due to decays inside the bubble chamber, rather than outside, because the π's and K's interact once they reach the absorber outside. The decay usually cannot be seen since the change in direction is extremely small, and as a result the decaying π (or K) is fitted along with the daughter μ as a single composite track. In bubble-chamber experiments, as opposed to electronic-counter experiments, only π's and K's from the primary interaction need to be considered as potential background sources.

We follow the same method used in a previous experiment[6] to calculate this background. We first determine the probability that decaying π's and K's can fake a muon using leaving-track measurements. This probability is calculated as a function of the momentum and the length of the track. Using the measured leaving-track momentum spectrum from a sample of 1400 CC events, one can thus estimate the total decay background. This procedure is followed separately for decays inside and outside the bubble chamber (for the latter, the probability is calculated as a function of momentum only).

To determine what fraction of decays would satisfy our muon identification criteria, we used a Monte Carlo program[40] which allowed leaving tracks to decay inside the bubble chamber, and fitted composite tracks to them (done separately for pion and kaon lifetimes and decay kinematics). The composite track and decay muon were extrapolated to the EMI, and their positions compared to calculate a two-plane confidence level. Only tracks with confidence level greater than 1% were considered as fake muons. Multiple Coulomb scattering effects were included in simulating the muon hit in the EMI. For calculating the probability for decays outside the bubble chamber, we assume that the decays take place just outside the bubble chamber (before the absorber) and that

they can be represented by decays taking place just inside the bubble-chamber wall (within 20 cm of the wall).

The final decay background estimate, shown in Table I, is calculated assuming[41] that 5% of the positive leaving tracks are due to protons and 6% to kaons (the rest being pions), whereas 8% of the negative leaving tracks are due to kaons (the rest being pions). The error on the background estimate is 20%; 10% is due to the uncertainty in the pion-to-kaon ratio in the leaving-tracks sample, and the rest is due to systematic differences in geometrical reconstruction among the various laboratories.

B. Punchthrough

We now estimate the background due to hadrons matching with hits in the EMI that are caused by (a) primary hadrons from the event which reach the EMI without interacting or decaying, (b) secondary, tertiary, etc., hadrons from the event (initiated by primary hadron interactions in the bubble chamber or the absorber), and (c) δ rays from the muon. These sources are collectively referred to as punchthrough.

The probability that a hadron can reach both EMI planes without interacting or decaying is extremely small, $\sim 5 \times 10^{-5}$, because of the presence of (typically) 10 interaction lengths of absorber. Therefore, the number of such hadrons in the present data sample of 13 300 charged-current events which can fake a muon is approximately 0.2; thus this source will be neglected.

The more important background is due to hadrons, both charged and neutral, which interact in the absorber giving rise to secondary and tertiary particles, some of which can hit EMIC. Some of these background hits can also be due to δ rays produced by the muon. A leaving track, other than the muon, which is predicted to hit EMIC can at times be associated with these background hits, thus making a good EMI match and faking a muon. To estimate this background, we use the actual hits in EMIC in the event time slot for detected CC events. We assume that the background hits, outside a small region around the extrapolated position of the leaving track, are spread uniformly along each of the axes of EMIC. Hits inside this small region are excluded to remove contributions from real dimuons and decays of pions and kaons. Using hits within 130 cm (65 cm) of the extrapolated position along the H (V) axis, we calculate a density of such background hits. Assuming that this density is the same within a region corresponding to a 1% cut on the two-plane confidence level, we can calculate the probability of a hit within this region. Summing this probability over all leaving tracks, other than the muons in CC events, with momentum above 4 GeV/c and with a good match in EMIB, we can thus estimate the total punchthrough

background. The final punchthrough background is given in Table I, along with 40% errors due to the estimation technique and statistical error from the number of tracks used in this calculation.

C. Accidental associations

It is possible for leaving tracks to match with hits in the EMI that are not caused, directly or indirectly, by particles from the event. Such tracks will be falsely labeled as muons. We estimate this background by using EMI information from a different frame. The total contribution is found to be less than 0.5 event for the entire dimuon sample and thus will be neglected.

V. ENERGY ESTIMATION OF THE DIMUON AND THE CHARGED-CURRENT SAMPLE

Because we do not detect all the neutral particles produced in an event, we have to correct the hadronic energy, and hence the incident neutrino energy. The charged-current sample required a larger correction than the dimuon event sample, because only the five highest-energy γ's and high-energy N^*'s were measured. To correct the dimuon event sample, we used a technique which has been used in previous experiments.[42] The longitudinal-momentum component of the visible hadronic shower (P_x) is corrected by a factor which is determined using the imbalance between the mean of the primary muon's transverse momentum (in the v-μ plane) and the mean transverse momentum of the hadronic shower in the same plane (the second muon is treated as part of this shower). The muon with the larger transverse momentum with respect to all the nonmuon particles coming from the primary vertex is labeled as the primary muon. The correction to the hadronic longitudinal momentum is written as

$$P_x^{\text{corr}} = b + a P_x ,$$

where $b = 4.8 \pm 2.0$ GeV/c and $a = 1.20 \pm 0.06$ (for both opposite- and like-sign-dilepton samples).

Using this technique on the neutrino charged-current events, we obtained the following values: $b = 2.5 \pm 0.3$ GeV/c and $a = 1.30 \pm 0.02$. However, even with these values, the average energy of the events was below that expected on the basis of the neutrino spectrum. To investigate the appropriateness of this correction for this event sample, we generated charged-current v events using a Monte Carlo program which simulated the measurement rules for these events, as mentioned in Sec. III. Figure 4 shows that the Monte Carlo CC events have some problem reproducing the visible hadronic energy spectrum, while Fig. 5 shows that they reproduce the muon-

TABLE I. Dimuon candidates and backgrounds (muon momenta ≥ 4 GeV/c).

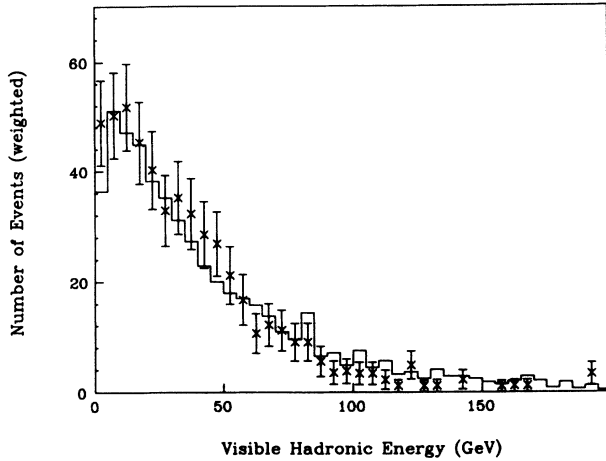|	$\mu^-\mu^-$	$\mu^-\mu^+$ and $\mu^+\mu^-$	$\mu^+\mu^+$
Events	11	52	1
π and K decays	6.6 ± 1.3	8.3 ± 1.4	0.5 ± 0.1
Punchthrough	3.0 ± 1.2	5.8 ± 2.1	0.3 ± 0.1
Net signal	1.4 ± 3.8	37.9 ± 7.6	0.2 ± 1.0

FIG. 4. Visible hadronic energy distribution for v-induced events for data (crosses) and the neutrino Monte Carlo simulation (histogram). The data correspond to 500 v CC events, taken from the measured event sample. The data are weighted by their electronic acceptance.

momentum spectrum for the CC sample rather well, confirming the input neutrino spectrum and the structure functions used. Therefore, it was decided to use the Monte Carlo simulation to determine the fractions of charged-current events in various energy bins. These are necessary to determine the dimuon–to–single-muon rate ratios as a function of energy (see below). For the total number of events and the estimation of backgrounds, the charged-current sample was used with the above-energy correction directly.

VI. EFFICIENCY AND RATES

Not all dimuon events produced in the bubble chamber are detected. There are losses due to scanning
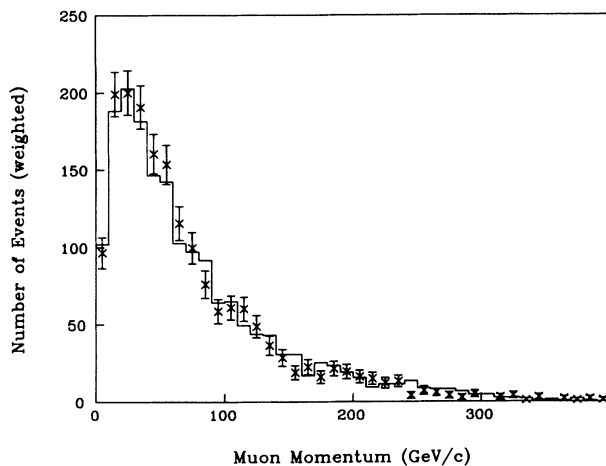
FIG. 5. The μ^- momentum distribution for CC events (crosses) and neutrino Monte Carlo simulation (histogram). The data correspond to 1790 μ^- tracks in a fully measured event and leaving-track sample. The data are weighted by their electronic acceptance.

inefficiencies, limited geometric and electronic acceptance of the EMI, and cuts made in the initial selection of the dimuon events.[38]

The geometric acceptance of the EMI for opposite-sign dimuons and like-sign dimuons with muon momenta above 4 GeV/c is $(83\pm2)\%$ and $(98\pm1)\%$, respectively (the EMI is asymmetric and detects μ^-'s better than μ^+'s). The acceptance for opposite-sign events is determined by using events generated by the charm Monte Carlo program (Sec. VII), whereas the acceptance for like-sign events is determined using the like-sign-dimuon candidates. The acceptance for v- and $\bar{v}$-induced charged-current events with muon momenta above 4 GeV/c is $(97\pm1)\%$ and $(92\pm2)\%$, respectively. The average electronic efficiency for detecting dimuons, including the instrumental efficiency of the EMI and the effect of the 1%-confidence-level cut, is $(80.6\pm0.8)\%$. It is determined using through-going muons that are generated in neutrino interactions upstream of the bubble chamber. The loss of dimuon events due to scanning inefficiencies (mainly due to faint photographs) and due to tracks overlooked or mismeasured is $(15\pm2)\%$, and the loss due to cuts made in the initial selection of dimuon events is $(16.0\pm1.8)\%$.

Thus, the total detection efficiency for opposite-sign events is $(48\pm2)\%$, and for like-sign events $(56\pm2)\%$. The total detection efficiency including geometric acceptance and instrumental efficiency for v- and $\bar{v}$-induced charged-current events is $(82\pm1)\%$ and $(77\pm2)\%$, respectively.

A. Opposite-sign events

Unless otherwise stated all results are for muon momenta above 4 GeV/c. The total rate for v- and $\bar{v}$-induced opposite-sign events, per charged-current event, is defined as

$$R = \frac{R(v+N\to\mu^-\mu^+X)+R(\bar{v}+N\to\mu^+\mu^-X)}{R(v+N\to\mu^-X)+R(\bar{v}+N\to\mu^+X)} .$$

We determine this rate, after subtracting background contributions and making efficiency corrections, to be $(0.62\pm0.13)\times10^{-2}$.

In order to calculate this rate separately for v- and $\bar{v}$-induced dimuons, we separate the two kinds of events assuming that the muon with the larger transverse momentum with respect to all the nonmuon particles coming from the primary vertex is the primary muon. According to the charm Monte Carlo simulation (described in Sec. VII), we expect to correctly identify 97% (95%) of the v-($\bar{v}$-) induced dimuons by this method. Using this separation method, we get 40 v-induced and 8 $\bar{v}$-induced opposite-sign dimuons, as shown in Fig. 6. Four events are on faint photographs and could not be measured completely, and are identified as v induced on the basis of the muon momenta transverse to the neutrino direction. This method has a selection efficiency similar to the one used above. Correcting these numbers, as mentioned above, we determine the opposite-sign rates to be
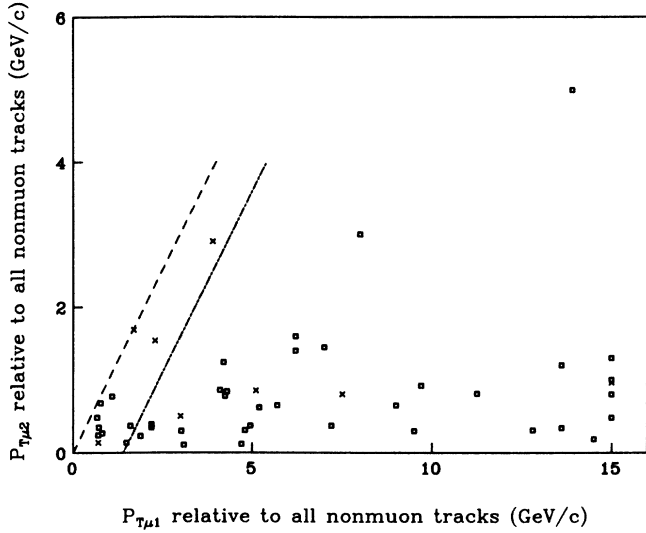
$P_{T\mu1}$ relative to all nonmuon tracks (GeV/c)

FIG. 6. Transverse momenta of the two muons for opposite-sign candidates with respect to all other particles in the event. The muon with the larger value of P_T is chosen as the primary muon. Squares indicate $\mu^-\mu^+$ events, and crosses $\mu^+\mu^-$ events. Primary muon momentum is along X axis. For events near the diagonal (between dashed lines, which are 1.4 GeV/c apart) the selection is ambiguous. For these ambiguous events on all other plots, we select the negative muon as the primary muon.

$$R^{-+} = \frac{R(\nu+N\rightarrow\mu^-\mu^+X)}{R(\nu+N\rightarrow\mu^-X)} = (0.64\pm0.14)\times10^{-2} ,$$

$$R^{+-} = \frac{R(\bar{\nu}+N\rightarrow\mu^+\mu^-X)}{R(\bar{\nu}+N\rightarrow\mu^+X)} = (0.47\pm0.25)\times10^{-2} .$$

On the basis of the 40 completely measured $\mu^-\mu^+$ events, R^{-+} is calculated in three energy bins to be $(0.30\pm0.14)\times10^{-2}$ for $E_\nu < 100$ GeV, $(0.81\pm0.28)\times10^{-2}$ for $100\le E_\nu < 200$ GeV, and $(0.93\pm0.29)\times10^{-2}$ for $E_\nu \ge 200$ GeV. See Fig. 7 for a comparison of our results with other experiments.

We observe eight neutral strange particles (V^0's) in the 52 opposite-sign events. However, to determine rates, we only use 48 events since four events are on faint photographs and could not be reliably scanned for V^0's (including event 22 560 104 in Table II). All V^0's are fit by a kinematic program (SQUAW). The characteristics of the
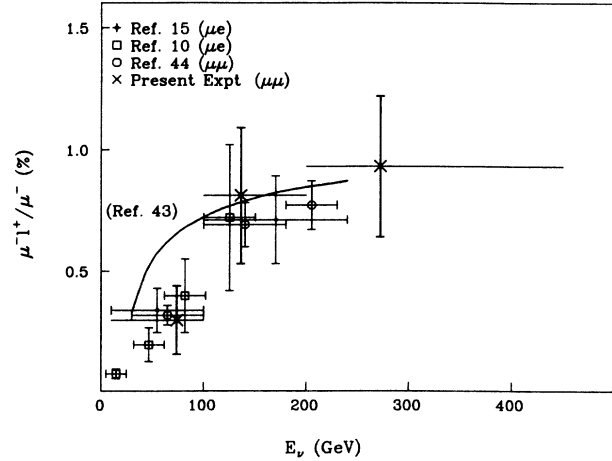

E_ν (GeV)

FIG. 7. The μ^-l^+/μ^- ($l^+=\mu^+$ or e^+) rate as a function of neutrino energy. The solid curve is the charm excitation curve due to Lai (Ref. 43), where the charm semileptonic branching ratio is taken to be 0.1 and no cut is made on the lepton momentum. For the experimental points, the momentum cut on the two leptons is 4 GeV/c in all cases except for Ref. 44 where it is 4.3 GeV/c.

V^0's are shown in Table II. All Λ/K ambiguities are treated as Λ's, except for the ambiguity in event 23 271 207 (this V^0 has no 3-constraint fit) which is assigned[45] an 80% probability of being a K^0. The raw $\mu\mu V^0X/\mu\mu X$ rate is $(15\pm5)\%$ (including background). We correct this rate for detection efficiency of the V^0's, K_S and Λ decay into neutral particles, and K_L decays. We weight each V^0 by the inverse of the probability that it will decay inside the bubble chamber. A zero weight is assigned if the V^0 decays within 1 cm of the primary vertex (poor detection efficiency) or within 20 cm of the downstream wall (poor momentum determination of the decay tracks). All dimuon events were examined by a physicist, and the scanning efficiency for V^0's which convert beyond 1 cm from the primary vertex is assumed to be 100%. We assume the same scan efficiency for V^0's in CC events. The V^0 weight also includes the (geometrical and electronic) probability of detecting the event in which it is found.

To estimate the V^0 rate in the background events, we use a sample of charged-current events which have at

TABLE II. Characteristics of V^0's for opposite-sign events.

Event	Type	V^0 type	χ^2 for K (3C) hypothesis	χ^2 for Λ (3C) hypothesis	Weight	Fitted Mom. (GeV/c)	$M_{\mu_2 V}$ (GeV/c^2)	No. of lifetimes
22 420 320	$\mu^-\mu^+$	K^0	2.6		2.12	0.3	3.50	1.00
22 560 104	$\mu^-\mu^+$	K^0	2.3		2.36	20.3	1.21	0.10
22 770 578	$\mu^+\mu^-$	Λ	14.3	1.1	1.46	2.8	3.30	0.36
22 830 011	$\mu^-\mu^+$	K^0	3.3		1.55	6.0	1.31	0.19
23 130 871	$\mu^-\mu^+$	Λ	6.0	0.4	4.59	3.1	2.70	0.14
23 161 895	$\mu^-\mu^+$	Λ	3.3	2.9	4.34	39.2	1.83	0.12
23 271 207	$\mu^-\mu^+$	K/Λ	0.4 (1C)	0.3 (1C)	1.57/1.64	4.3	2.20	1.51/1.1
23 321 255	$\mu^-\mu^+$	Λ		6.7	1.76	0.6	3.40	1.4

least two leaving tracks. For each event we calculate the probability that it could fake a dimuon event by summing the decay and punchthrough probabilities over all leaving hadronic tracks in the event. The V^0 content of the background events is calculated by adding up the background probabilities of all events containing V^0's. The raw V^0 fraction in the background events is $(10.2\pm1.8)\%$, while the raw V^0 fraction in the complete charged-current sample is $(10.5\pm1.0)\%$. Subtracting background, correcting for detection efficiencies and unseen decays, we calculate the corrected V^0 rate per opposite-sign-dimuon event to be 0.65 ± 0.29.

The neutral-strange-particle rate in opposite-sign-dimuon events agrees with the hypothesis that such events are due to the production of a charm quark and its subsequent decay. This result is also in agreement with the corrected V^0 rate of 0.6 ± 0.2 in μe events[10] (mean energy of ν-induced CC events ~ 30 GeV) and 0.6 ± 0.3 in $\mu\mu$ events[6] (mean energy of ν-induced CC events ~ 90 GeV).

B. Like-sign dimuons

The number of like-sign-dimuon candidates is consistent with the expected number of background events, as can be seen in Table I. We calculate the 90%-C.L. upper limit on the ratio $\mu^-\mu^-/\mu^-\mu^+$ to be 0.2. The 90%-C.L. upper limit for $\mu^-\mu^-/\mu^-$ is 1.2×10^{-3}, and on the basis of one $\mu^+\mu^+$ event we set the 90%-C.L. upper limit for $\mu^+\mu^+/\mu^+$ at 2.5×10^{-3}. Dividing the $\mu^-\mu^-$ data into two energy bins: the 90%-C.L. upper limit for $E_\nu < 200$ GeV is 6.8×10^{-4}; and, for $E_\nu \geq 200$ GeV, 4.2×10^{-3}. For $E_\nu \geq 200$ GeV we observe seven $\mu^-\mu^-$ events, which is consistent with the estimated background of 4.3 ± 1.3 events. Interpreting the excess 2.7 events as a signal would imply a rate of
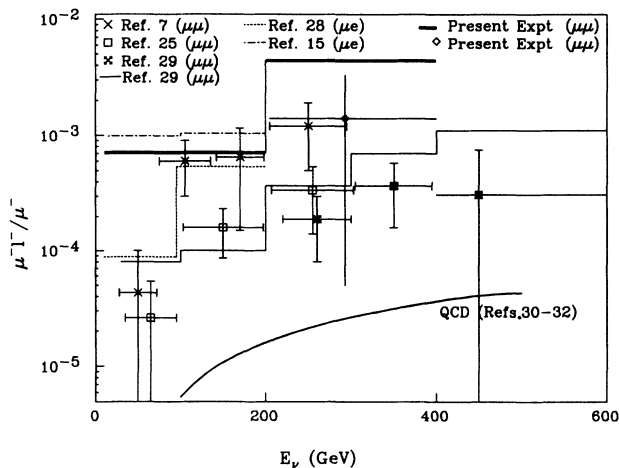
$(1.40^{+1.90}_{-1.35})\times10^{-3}$ in this energy bin. From these results we conclude that there is no evidence for prompt like-sign-dimuon production at any energy. See Fig. 8 for a comparison of our results with other experiments.

In order to compare our results more directly with those of counter experiments, we also studied the like-sign-dimuon candidates after making a 9-GeV/c cut on the muon momenta. We observe six $\mu^-\mu^-$ events with an estimated background of 4.3 ± 1.0 events. The 90%-C.L. upper limit on the ratio $\mu^-\mu^-/\mu^-$ is 1.1×10^{-3}.

There is one V^0 in the like-sign event sample. This corresponds to a raw V^0 rate of $(8.3^{+12.9}_{-5.1})\%$. In comparison, the raw V^0 rate in charged-current events is $(10.5\pm1.0)\%$, and in like-sign background events, it is $(7.8\pm1.8)\%$. Thus, in the like-sign-dimuon sample, there is no evidence of an excess of V^0's over that found in charged-current events.

VII. COMPARISON OF OPPOSITE-SIGN DATA SAMPLE WITH CHARM MONTE CARLO SIMULATION

In Figs. 9–20 we plot various kinematical variables for the opposite-sign data sample and compare them with distributions generated by a charm Monte Carlo simulation.[6] The contribution of background events in the dimuon sample is taken into account using the CC sample. Each CC event is weighted by the punchthrough and decay probabilities summed over all the hadronic leaving tracks. The charm Monte Carlo simulation is normalized to the net dimuon signal, and the background predictions are normalized to the number of background events in the sample. The means of some of the kinematical vari-
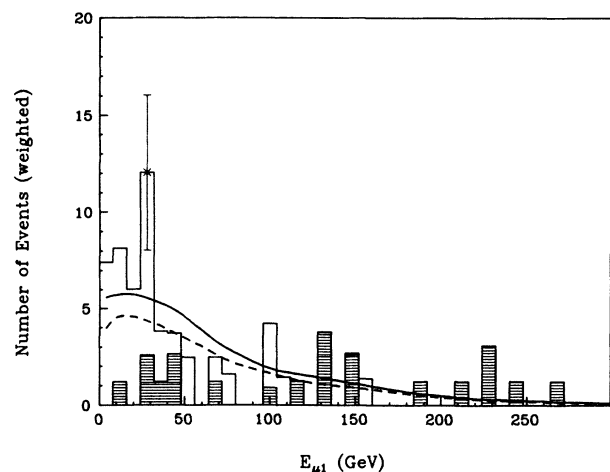

FIG. 8. The μ^-l^-/μ^- rate as a function of neutrino energy. The solid curve is from first-order perturbative QCD calculations (Refs. 30–32). The solid and broken horizontal lines, and the box (parallel to the X axis) are 90%-C.L. upper limits. The momentum cut on the two leptons is 9 GeV/c in Refs. 25 and 29, 10 GeV/c in Ref. 7, and 4 GeV/c in the present experiment. In Ref. 28, $P_\mu \geq 5$ GeV/c and $P_e \geq 4$ GeV/c, whereas in Ref. 15, $P_\mu \geq 4$ GeV/c and $P_e \geq 0.8$ GeV/c.

FIG. 9. Energy distribution of the primary muon for opposite-sign candidates. The Y axis corresponds to the number of opposite-sign candidates (weighted for geometrical and instrumental acceptance). The dashed curve is the Monte Carlo prediction for opposite-sign events (normalized to the net dimuon signal), and the solid curve is the sum of Monte Carlo and background predictions (the latter normalized to the total number of background candidates in the sample). Candidates with energy above 200 GeV are shaded. The same convention is followed in Figs. 10 and 12–20.
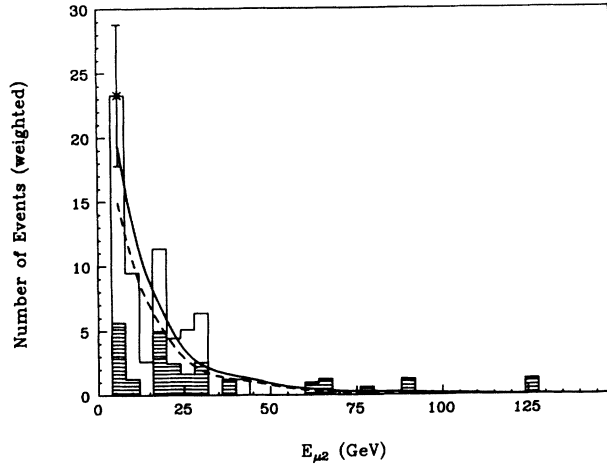
FIG. 10. Energy distribution of the secondary muon for opposite-sign candidates.
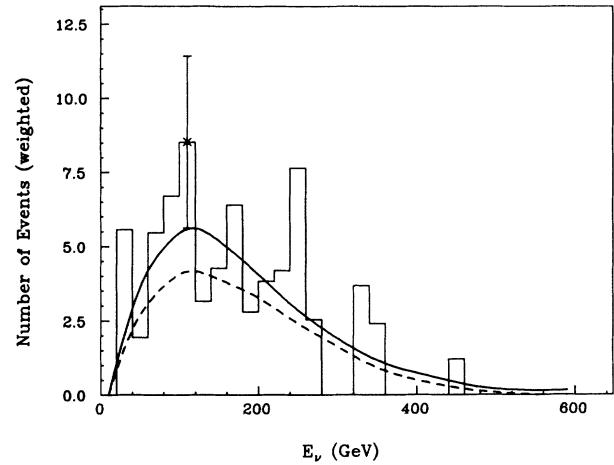

FIG. 11. Neutrino energy distribution for opposite-sign candidates.

ables for various event samples are presented in Table III. We use the previously mentioned 48 completely measured opposite-sign events in these plots and tables.

In the following distributions, in order to better identify the primary muon in dimuon events, we label an event as a $\mu^+\mu^-$, signifying a $\bar{\nu}$-induced dimuon event, only if the transverse momentum of the μ^+ with respect to all nonmuonic tracks in the event is greater than that of the μ^- by at least 1.4 GeV/c (this number is determined using the charm Monte Carlo simulation).

In the following plots, contributions from events with reconstructed energies above 200 GeV are shown shaded. The means of some kinematic variables for events with energy above 200 GeV are presented in Table IV. In the present sample, 18 out of 48 [(36.0±8.5)%] well-measured events have energy above 200 GeV. According to the charm Monte Carlo simulation, we expect (34.5±1.0)% of the events to have energies above 200 GeV.

Our charm Monte Carlo program has been described elsewhere.[6,38] The basic assumptions regarding charm production in the Monte Carlo program are (1) a c ($\bar{c}$) quark is produced via ν ($\bar{\nu}$) interactions with a d ($\bar{d}$) or a s ($\bar{s}$) quark, (2) the quark structure functions are based upon results obtained by the CERN-Dortmund-Heidelberg-Saclay (CDHS) experiment.[8] The valence-quark distribution is represented by $x^{0.5}(1-x)^{3.5}$, and the sea-quark distribution is represented by $(1-x)^{7.0}$. The sea is not SU(3) symmetric, and the ratio $2S/(\bar{U}+\bar{D})$ is taken to be 0.52 (Ref. 8). (3) The charm fragmentation function is taken to be of the form of Peterson et al.:[46]

$$D_c(z) = \frac{1}{z[1-1/z-\epsilon/(1-z)]^2},$$

where $\epsilon = 0.16$ (Ref. 47). (4) The charm quark hadronizes to D and D^* mesons (in the ratio 3:2) (Ref. 48), and if a D^* is produced it is allowed to decay to $D\pi$ or $D\gamma$ in the

TABLE III. Average values of kinematic quantities for opposite-sign events.

	Dimuon sample (weighted)	Background (weighted)	Dimuons (weighted) (sample−bkgd)	Dimuon Monte Carlo simulation
$E_{\mu1}$ (GeV)	69.8±9.5	73.3±6.3	68.9±11.0	75.0±2.2
$E_{\mu2}$ (GeV)	20.6±2.9	21.9±2.0	20.2±3.5	20.2±0.7
E_ν (GeV)	168±14	187±10	162±14	172±3
γ	0.36±0.06	0.44±0.03	0.33±0.07	0.45±0.01
$\beta=E_{\mu2}/E_{\mu1}$	0.61±0.15	0.63±0.10	0.61±0.17	0.64±0.03
x	0.19±0.02	0.17±0.01	0.20±0.02	0.16±0.01
y	0.62±0.03	0.60±0.02	0.63±0.03	0.57±0.01
W (GeV/c^2)	11.6±0.6	12.4±0.3	11.3±0.6	11.6+0.2
Q^2 (GeV/c)^2	33.2±5.2	30.8±3.5	34.0±5.8	28.9±1.3
$M_{\mu\mu}$ (GeV/c^2)	3.6±0.4	3.2±0.2	3.7±0.4	3.0±0.1
Φ (deg)	128±6.5	134±4	126±7	135±2.0
$P_{\perp\mu2}$ (GeV/c)[a]	0.36±0.04	0.34±0.02	0.37±0.05	0.30±0.0
Charged mult	8.0±0.5	7.9±0.3	8.0±0.6	
$z_{\mu2}$	0.23±0.02	0.24±0.01	0.23±0.02	0.23±0.00 (Peterson)

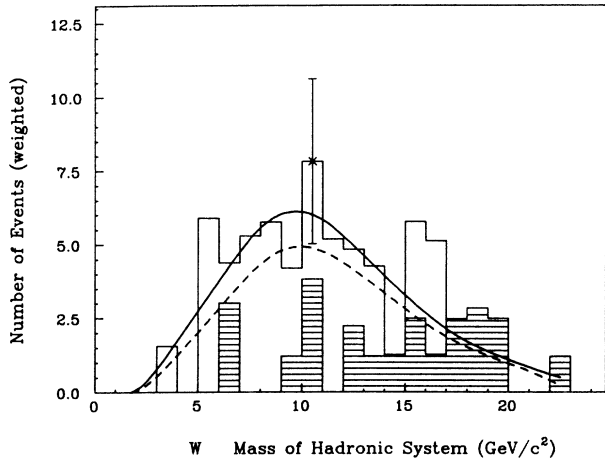[a]Momentum of the second muon perpendicular to the μ-ν plane.

FIG. 12. Invariant-mass W distribution of the hadronic system (including the secondary muon) for opposite-sign candidates.
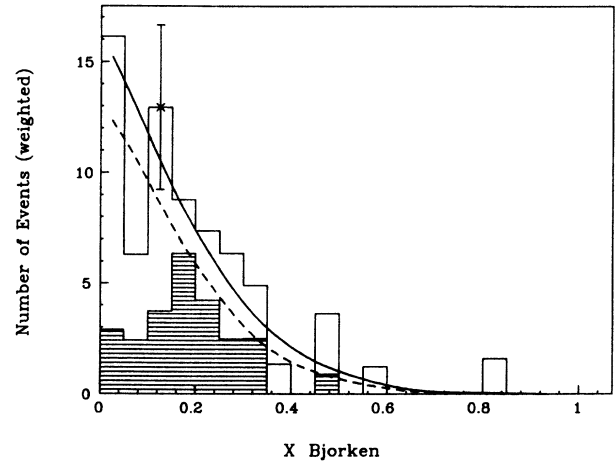

FIG. 14. Bjorken-x distribution for opposite-sign-dimuon candidates. $x = Q^2/2M_N\nu$, where Q^2 is the four-momentum transfer squared, M_N is the nucleon mass, and $\nu = E_\nu - E_{\mu 1}$.

ratio 2:1 (Ref. 49). (5) The D meson has three decay modes, $\pi\mu\nu$, $K\mu\nu$, and $K^*\mu\nu$ with branching ratios 0.06/0.47/0.47 (Ref. 8).

In the following plots, the events are weighted by the inverse of their electronic and geometric acceptances. In Figs. 9–11 we present the plots for the energy of the primary and secondary muons and the event energy. In these and the following figures, the dashed curves represent the Monte Carlo predictions, and the sum of Monte Carlo and background predictions is represented by the solid curves. Figures 12 and 13 show the distributions for the mass of the hadronic system (including the secondary muon) and for the four-momentum-transfer squared.

In Fig. 14, we show the Bjorken-x distribution. There appears to be a lack of events at low x with energy above 200 GeV, but the statistical significance of the deficiency is less than 2 standard deviations.

The y distribution is shown in Fig. 15. The lack of events at low y is attributable to the charm threshold suppression and the slight depletion of events at very high y is attributable to the momentum cut of 4 GeV/c on the primary muon. At $0.8 \le y \le 0.9$ there is an accumulation of 23 weighted events, while the prediction from the charm Monte Carlo simulation plus background is ten events. The 23 weighted events correspond to 15 actual events. Multiplying the Monte Carlo prediction by the average acceptance for dimuon events, we would expect 6.7 actual events. The Poisson probability of 6.7 yielding 15 or more is 0.4%. For $y \ge 0.8$, 19 actual events are observed compared with 10.9 predicted. The Poisson probability of 10.9 yielding 19 or more is 1.7%, which corresponds to less than 3 standard deviations. Such a fluctuation is not unlikely when one considers the number of plots and bins examined. The 15 events in the $0.8 \le y \le 0.9$ region contain four Λ's and one K^0, where
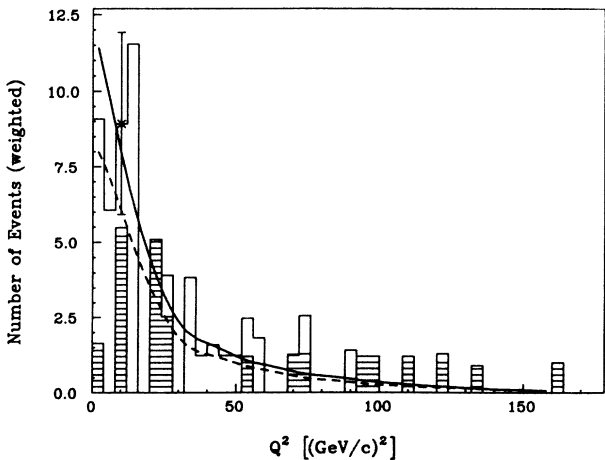

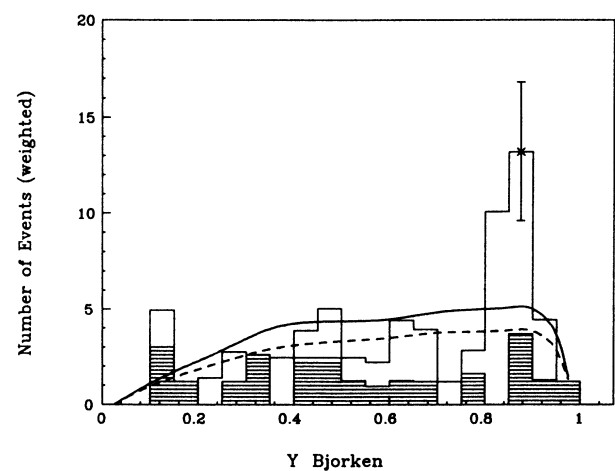FIG. 13. The four-momentum transfer squared distribution Q^2 for opposite-sign-dimuon candidates.

FIG. 15. Bjorken-y distribution for opposite-sign-dimuon candidates, where $y = \nu/E_\nu$.
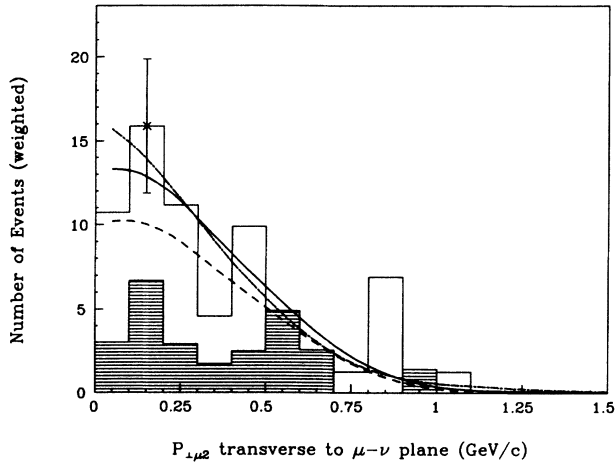
FIG. 16. Momentum distribution of the second muon in a direction perpendicular to the plane formed by μ_1 and the incident ν (for opposite-sign-dimuon candidates). The dotted-dashed curve corresponds to hadrons with momentum above 4 GeV/c in the charged-current sample, while the other two curves have the meanings given above.

the whole sample (48 events) has four Λ's and four K^0's.

We have checked that the accumulation is not due to our analysis methods or to poorly measured tracks. For instance, when an alternate method was used to select the primary muon (using the transverse momenta of the muons relative to the neutrino direction rather than the hadron direction), the enhancement remained. When the data were analyzed with no energy correction, the enhancement broadened and moved to slightly lower y.

We have examined the other distributions for the 15 events with $0.8 \leq y \leq 0.9$ and find no other obvious accumulation of these events that is not directly attributable to the variable's correlation with y. Some mean values are given in Table V. The distributions of missing trans-

verse momentum, both in and out of the plane, look similar to those of the total sample. This similarity argues against the accumulation resulting from some neutral-current process (except at very small x values).

We have also compared properties of the 15 events with those of charm Monte Carlo events that have $0.8 \leq y \leq 0.9$. Mean values are given in Table V. There is fair agreement between the two samples, and for no variable is the difference in the mean values more than 2.5 standard deviations.
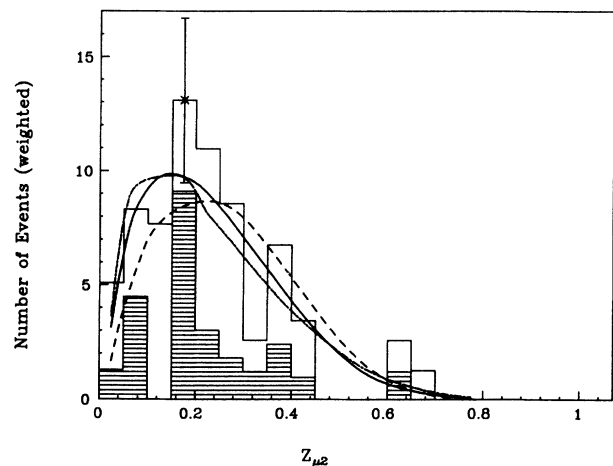
The accumulation appears to be in the low-energy

FIG. 17. Charged-hadron multiplicity distribution for opposite-sign candidates. The dashed-dotted curve corresponds to the charged-current sample.
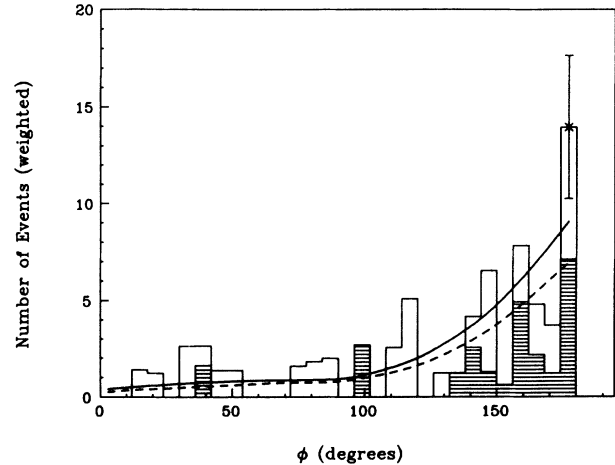
FIG. 18. Distribution of the angle Φ between the two muons, projected on a plane perpendicular to the neutrino direction (for opposite-sign-dimuon candidates).

FIG. 19. Distribution of the fraction $z_{\mu2} = E_{\mu2}/\nu$ of the hadronic energy carried by the second muon, for opposite-sign candidates. The solid (Monte Carlo and background predictions) curve correspond to the Peterson function for the charm fragmentation function, whereas the dashed-dotted line corresponds to the sum of Monte Carlo and background predictions for a uniform z distribution, and the dashed line corresponds to Monte Carlo plus background predictions for a δ function, $\delta(z - 0.68)$.
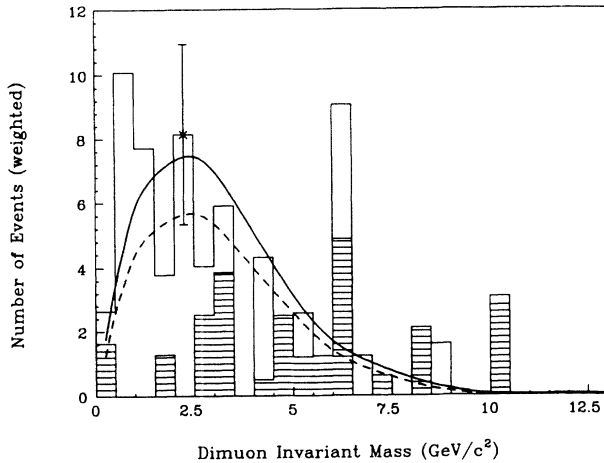
FIG. 20. Invariant-mass distribution for the two muons for opposite-sign-dimuon candidates.

FIG. 22. Energy distribution of the second muon for like-sign-dimuon candidates.

(below 200 GeV) events. No accumulation was seen in previous low-energy experiments.[6,8] The events' energies are estimated assuming that they are conventional charged-current events. The events could be high energy, with missing energetic neutrals, but the small missing transverse momentum noted above constrains them to lie close to the beam direction. No similar accumulation is seen in another experiment in the same beam with the same energy;[50] but we note that their analysis has a muon momentum cut of 9 GeV/c. The probability that our model gives as many events as the data for $y \geq 0.8$ is 1.7%.

Figure 16 shows the momentum distribution of the

second muon perpendicular to the μ_1-ν plane. The dotted-dashed curve corresponds to hadrons with momentum above 4 GeV/c in the charged-current sample, whereas the other two curves have the meanings mentioned above. In Fig. 17 we present the charged-particle multiplicity distribution. The dotted-dashed curve is obtained from charged-current events. Figure 18 shows the distribution of the angle between the two muons projected on a plane perpendicular to the neutrino direction.

In Fig. 19 we show the fraction of the hadronic energy carried off by the secondary muon, $z_{\mu2} = E_{\mu2}/(E_\nu - E_{\mu1})$. This variable measures the charm fragmentation function indirectly, since the second muon carries only part of the charmed hadron momentum. For comparison, $z_{\mu2}$ curves obtained using (in the charm Monte Carlo simulation) three different charm fragmentation functions are plotted. The solid curve is the sum of the background and charm Monte Carlo predictions using the Peterson

FIG. 21. Energy distribution of the primary muon for like-sign-dimuon candidates. The Y axis corresponds to the number of events (weighted for geometrical and electronic acceptance) in the dimuon sample. The solid line is the background prediction, normalized to the total number of background events. The same convention is followed in Figs. 22–30.
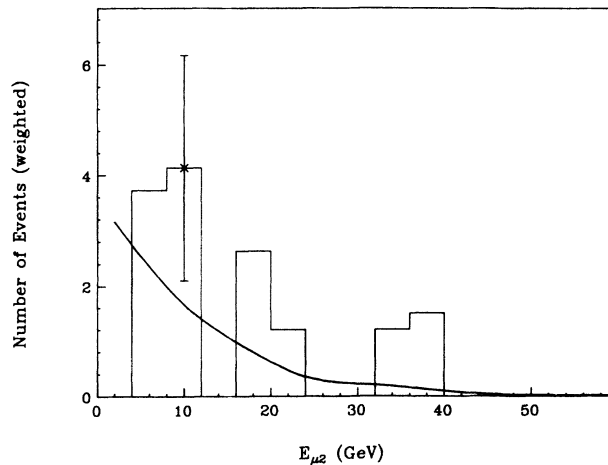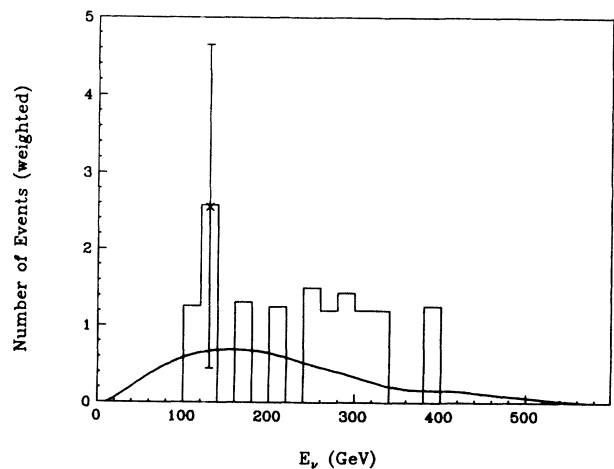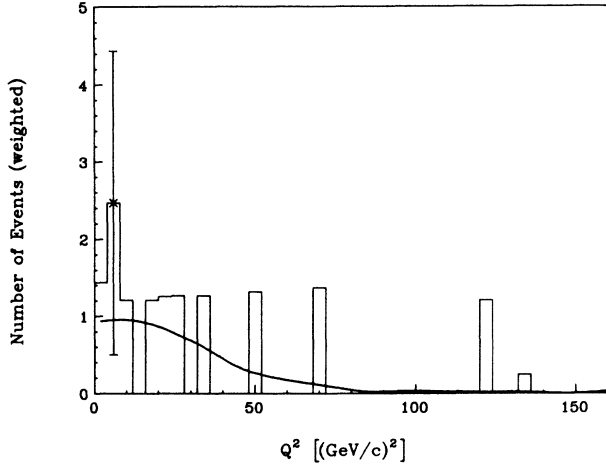

FIG. 23. Neutrino energy distribution for like-sign-dimuon candidates.

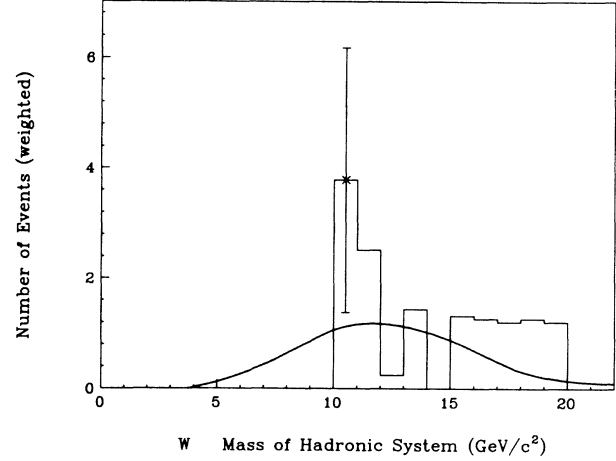FIG. 24. Four-momentum transfer squared distribution for like-sign-dimuon candidates.

FIG. 25. Invariant-mass W distribution of the hadronic system (including the secondary muon), for like-sign-dimuon candidates.

et al.[46] charm fragmentation function. The dotted-dashed curve uses a uniform z distribution for the charm fragmentation, and the dashed line is obtained using a delta function, $\delta(z - 0.68)$. The background is the same in all these curves.

In Fig. 20 we present the invariant-mass $M_{\mu\mu}$ plot for the two muons. The small peak at 10 GeV/c^2 is due to one high weight event. The larger peak at 6.4 GeV/c^2 is composed of seven events. However, the error on the invariant masses of these events is rather large (all but one have errors greater than 1 GeV/c^2, where the bin width is 0.5 GeV/c^2). If instead we look at a mass range from 5.0 to 7.5 GeV/c^2, the observed 14.6 weighted events are less than 2 standard deviations above the predicted 8.4 events.

In general the charm Monte Carlo and background predictions agree with the dimuon data sample. Howev-

er, there is an accumulation of events for $0.8 \leq y \leq 0.9$. This accumulation is not seen by other experiments at lower energies or at the same energy, and the probability that the model gives as many events as the data for $y \geq 0.8$ is 1.7%. The general agreement between data and Monte Carlo simulation leads us to believe that we do not have any systematic biases in selecting dimuon candidates, and thus we can use the same selection criteria to tag like-sign candidates with confidence.

VIII. COMPARISON OF THE LIKE-SIGN DATA SAMPLE WITH BACKGROUND PREDICTIONS

In Figs. 21–30, the histogram represents the like-sign candidates and the solid curve corresponds to back-

TABLE IV. Average values of kinematic quantities for opposite-sign events with energy above 200 GeV.

	Dimuon sample (weighted) (incl. bkgd.)	Dimuon Monte Carlo simulation
$E_{\mu1}$ (GeV)	127.5±16.0	131.0±2.5
$E_{\mu2}$ (GeV)	32.2±6.1	30.0±0.8
E_ν (GeV)	273.0±12.0	284.0±2.0
γ	0.49±0.1	0.52±0.01
$\beta = E_{\mu2}/E_{\mu1}$	0.42±0.14	0.58±0.03
x	0.19±0.02	0.17±0.01
y	0.54±0.05	0.54±0.01
Q^2 [(GeV/c)^2]	52.1±9.3	45.8±1.5
W (GeV/c^2)	14.3±0.9	14.8±0.1
$M_{\mu\mu}$ (GeV/c^2)	5.3±0.6	3.9±0.1
Φ (deg)	148.0±7.2	142.0±1.2
$P_{\perp\mu2}{}^a$ (GeV/c)	0.36±0.05	0.28±0.01
$Z_{\mu2}$	0.22±0.03	0.21±0.00

[a]Momentum of the second muon perpendicular to the μ-ν plane.

TABLE V. Average values of kinematic quantities of the $0.8 \leq y \leq 0.9$ opposite-sign dimuon events.

Quantity	15 events with $0.8 \leq y \leq 0.9$	Charm Monte Carlo events with $0.8 \leq y \leq 0.9$
$E_{\mu1}$ (GeV)	19.6±2.9	24.2
$E_{\mu2}$ (GeV)	18.8±4.3	27.5
E_ν (GeV)	134±21	162
x	0.16±0.03	0.16
Q^2 [(GeV/c)^2]	41±12	39.9
W (GeV/c^2)	12.6±1.0	14.0
$M_{\mu\mu}$ (GeV/c^2)	2.3±0.5	2.7
Φ (deg)	96±12	124
$P_{\perp\mu2}{}^a$ (GeV/c)	0.48±0.08	0.31
$Z_{\mu2}$	0.18±0.03	0.21

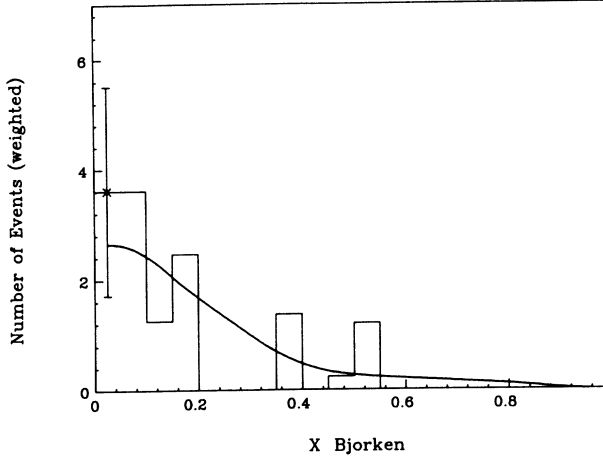[a]Momentum of the second muon perpendicular to the μ-ν plane.

FIG. 26. Bjorken-x distribution for like-sign-dimuon candidates. $x = Q^2/2M_N \nu$, where Q^2 is the four-momentum transfer squared, M_N is the nucleon mass, and $\nu = E_\nu - E_{\mu 1}$.
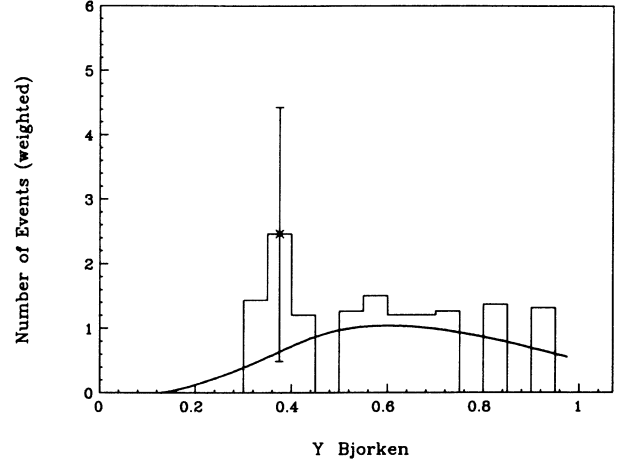

FIG. 27. Bjorken-y distribution for like-sign-dimuon candidates, where $y = \nu/E_\nu$.

ground predictions. The background in the dimuon sample is estimated using the CC sample (as determined in the present experiment). Each CC event is weighted by the punchthrough and decay probabilities summed over all the hadronic leaving tracks. As before, the primary and secondary muons are chosen on the basis of their momentum transverse to all the nonmuon particles in the event. In all but one case, the primary muon's transverse momentum is greater than that of the secondary muon by at least 2 GeV/c. The means of the kinematic variables are shown in Table VI, and characteristics of each event are shown in Table VII.

In Figs. 21 and 22 we show the distributions for the energy of the primary and secondary muons. In Fig. 23 we plot the energy of the incident neutrino. In the data there are no events with $E_\nu < 100$ GeV, whereas the background calculation, described in Sec. IV, predicts that we should see 3 ± 1 events. Figure 24 shows the Q^2 distribu-

tion, and Fig. 25 shows the invariant-mass plot of the hadronic system, W. There are no events in the data for $W < 10$ GeV/c^2. Figures 26 and 27 show the Bjorken-x and -y distributions. Figure 28 shows the fraction of the hadronic energy carried off by the second muon. In Fig. 29 we show the distribution of the angle between the two muons projected on a plane perpendicular to the neutrino direction. The peaking of this distribution near 180° shows that the two muons are anticorrelated, and that the second muon is associated with the hadron shower. In Fig. 30 we show the transverse-momentum distribution of the second muon with respect to the hadron shower, where the latter is determined from the direction of the neutrino beam and the leading muon. This transverse momentum is limited to small values, as is the transverse momentum with respect to the plane defined by the incoming neutrino and the primary muon (not shown). There is no discrepancy between the data and

TABLE VI. Average values of kinematic quantities for like-sign events.

	Event sample (weighted)	Background sample (weighted)
$E_{\mu 1}$ (GeV)	103 ± 19	77 ± 7
$E_{\mu 2}$ (GeV)	16.4 ± 3.2	17.4 ± 2.2
E_ν (GeV)	235 ± 25	194 ± 11
Q^2 [(GeV/c)^2]	35 ± 10	40.4 ± 3.7
W (GeV/c^2)	14 ± 1	12.7 ± 0.5
$M_{\mu\mu}$ (GeV/c^2)	2.9 ± 0.5	3.2 ± 0.2
x	0.16 ± 0.05	0.20 ± 0.02
y	0.58 ± 0.06	0.61 ± 0.02
Φ (deg)	124 ± 13	136 ± 5
$P_{\perp\mu2}$[a] (GeV/c)	0.37 ± 0.09	0.28 ± 0.03
Charged multiplicity	9.8 ± 1.7	9.1 ± 0.4
$z_{\mu2}$	0.14 ± 0.03	0.16 ± 0.01

[a]Momentum of the second muon perpendicular to the μ-ν plane.
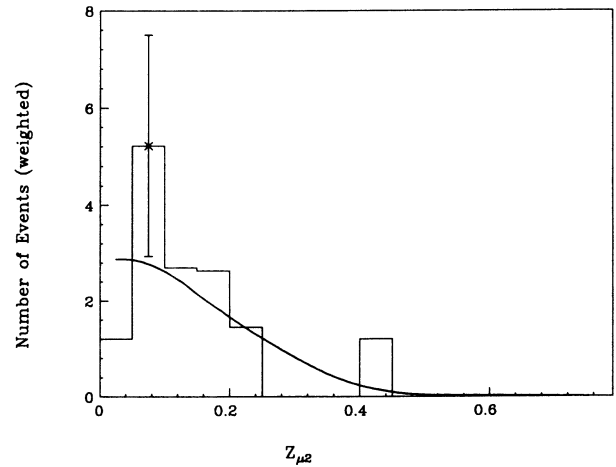

FIG. 28. Distribution of the fraction $z_{\mu2} = E_{\mu2}/\nu$ of the hadronic energy carried away by the second muon for like-sign candidate events.
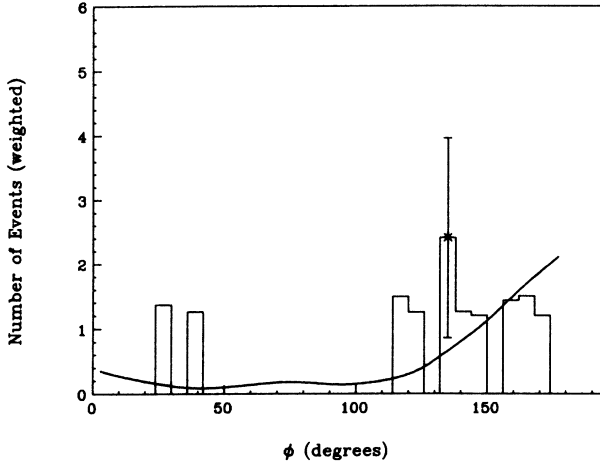
FIG. 29. Distribution of the angle Φ between the two muons, projected on a plane perpendicular to the neutrino direction (for like-sign-dimuon candidates).
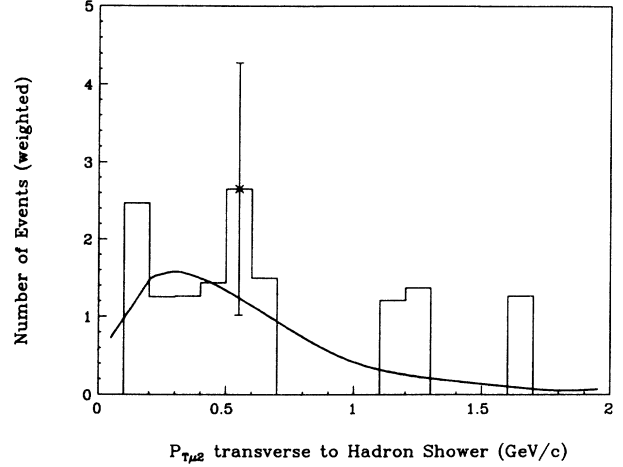

FIG. 30. Momentum distribution of the second muon, transverse to the hadron shower, where the latter is determined using the direction of the neutrino beam and the leading muon (for like-sign-dimuon candidates).

background, in contrast with such indications from a previous experiment.[34] We conclude that the like-sign sample is consistent with background.

IX. CONCLUSIONS

We have reported results on dimuon events from an exposure of the 15-ft bubble chamber to a quadrupole triplet neutrino beam at the Fermilab Tevatron, where we identified 52 opposite-sign-dimuon and 12 like-sign-dimuon candidates.

The like-sign sample is consistent with background both in rate and distributions of kinematic quantities. Background estimates are based on charged-current hadron distributions and muon detection efficiencies which are measured in the same experiment. After accounting for the background contribution and detection

efficiencies, the 90%-C.L. upper limit for the ratio $\mu^-\mu^-/\mu^-$ is 1.2×10^{-3}, for $P_\mu \geq 4$ GeV/c, and 1.1×10^{-3} for events with $P_\mu \geq 9$ GeV/c. Dividing the $\mu^-\mu^-$ data into energy bins, the 90%-C.L. upper limit, for muon momenta above 4 GeV/c, for $E_\nu < 200$ GeV is 6.8×10^{-4}, and for $E_\nu \geq 200$ GeV, the upper limit is 4.2×10^{-3}.

For the opposite-sign sample, after subtracting background and correcting for detection losses, we measure the ratios $\mu^-\mu^+/\mu^-$ and $\mu^+\mu^-/\mu^+$, for $P_\mu \geq 4$ GeV/c, to be $(0.64\pm0.14)\%$ and $(0.47\pm0.25)\%$, respectively. We further divide the ν-induced opposite-sign events into three energy bins and determine $\mu^-\mu^+/\mu^-$: (1) $(0.30\pm0.14)\%$ for $E_\nu < 100$ GeV, (2) $(0.81\pm0.28)\%$ for $100 \leq E_\nu < 200$ GeV, and (3) $(0.93\pm0.29)\%$ for $E_\nu \geq 200$ GeV.

We observe eight V^0's in the opposite-sign sample. After subtracting background and correcting for detec-

TABLE VII. Details of individual like-sign events.

Event	Potential length (cm)	$P_{\mu1}$ (GeV/c)	$P_{\mu2}$ (GeV/c)	E_{vis} (GeV)	$P_{T\mu1}$[a] (GeV/c)	$P_{T\mu2}$[a] (GeV/c)
22 370 766	200	104.0	34.1	238.0	5.4	0.4
22 390 301	117	19.0	17.2	100.0	3.5	0.8
22 430 214[b]	192	112.0	18.9	225.0	2.5	0.3
22 550 842	116	125.0	5.0	191.0	9.6	0.2
22 600 767	256	197.0	10.5	278.0	3.3	0.4
22 700 893	170	103.0	36.5	225.0	10.6	0.8
22 711 047	294	99.0	8.4	266.0	2.8	0.5
22 810 988	130	28.0	6.1	94.0	3.0	0.3
23 001 232	253	209.0	7.8	308.0	20.2	0.6
23 271 195	201	177.0	36.8	348.0	5.9	2.2
23 330 068	121	77.0	23.5	125.0	7.9	2.6
23 330 872	107	8.8	10.4	135.0	1.8	0.7

[a]Momentum transverse to nonmuon tracks in event.
[b]$\mu^+\mu^+$ event.

tion losses we determine the average number of neutral-strange particles per dimuon event to be 0.65 ± 0.29. In the case of the like-sign-dimuon sample, there is no evidence for any excess of V^0's over that produced in charged-current events.

We compare kinematical distributions for the opposite-sign sample with the predictions of a charm production and decay Monte Carlo simulation. The agreement of distributions is good except for the y distribution where there is an accumulation of events for $0.8 \leq y \leq 0.9$, and after checking our and other experiments, we have no satisfactory explanation for this other than a statistical fluctuation.

ACKNOWLEDGMENTS

*Now at Syracuse University, NY.

†Now at Johns Hopkins University, Baltimore, MD.

‡Now at Rutherford Appleton Laboratory, UK.

§Also at Universitaire Instelling Antwerpen, B-2610 Wilrijk, Belgium.

**Now at Fermilab, Batavia, IL.

††Now at University of Ferrara, Ferrara, Italy.

‡‡At Seton Hall University, S. Orange, NJ.

§§Now at Tufts University, Medford, MA.

[1]A. Benvenuti et al., Phys. Rev. Lett. **34**, 419 (1975).

[2]M. Holder et al., Phys. Lett. **69B**, 377 (1977).

[3]P. C. Bosetti et al., Phys. Lett. **73B**, 380 (1978).

[4]N. Armenise et al., Phys. Lett. **86B**, 115 (1979).

[5]N. Armenise et al., Phys. Lett. **94B**, 527 (1980).

[6]H. C. Ballagh et al., Phys. Rev. D **21**, 569 (1980).

[7]T. Trinko et al., Phys. Rev. D **23**, 1889 (1981).

[8]H. Abramowicz et al., Z. Phys. C **15**, 19 (1982).

[9]G. Gerbier et al., Z. Phys. C **29**, 15 (1985).

[10]C. Baltay et al., Phys. Rev. Lett. **39**, 62 (1977).

[11]H. C. Ballagh et al., Phys. Rev. Lett. **39**, 1650 (1977).

[12]O. Erriquez et al., Phys. Lett. **77B**, 227 (1978).

[13]M. Murtagh, in Proceedings of the International Symposium on Lepton and Photon Interactions at High Energies, Batavia, Illinois, 1979, edited by T. B. W. Kirk and H. D. I. Abarbanel (Fermilab, Batavia, Illinois, 1980).

[14]J. P. Berge et al., Phys. Lett. **81B**, 89 (1979).

[15]H. C. Ballagh et al., Phys. Rev. D **24**, 7 (1981).

[16]A. Haatuft et al., Nucl. Phys. **B222**, 365 (1983).

[17]P. Marage et al., Z. Phys. C **21**, 307 (1984).

[18]N. J. Baker et al., Phys. Rev. D **32**, 531 (1985).

[19]V. V. Ammosov et al., Z. Phys. C **35**, 329 (1987).

[20]V. V. Ammosov et al., Z. Phys. C **40**, 493 (1988).

[21]A. Benvenuti et al., Phys. Rev. Lett. **41**, 1204 (1978).

[22]V. V. Ammosov et al., Phys. Lett. **106B**, 151 (1981).

[23]M. Jonker et al., Phys. Lett. **107B**, 241 (1981).

[24]K. Nishikawa et al., Phys. Rev. Lett. **54**, 1336 (1985).

[25]H. Burkhardt et al., Z. Phys. C **31**, 39 (1986).

[26]K. Lang et al., Z. Phys. C **33**, 483 (1987).

[27]V. V. Ammosov et al., Phys. Lett. B **189**, 245 (1987).

[28]C. Baltay et al., Phys. Rev. Lett. **55**, 2543 (1985).

[29]B. A. Schumm et al., Phys. Rev. Lett. **60**, 1618 (1988).

[30]B. L. Young et al., Phys. Lett. **74B**, 111 (1978).

[31]K. Hagiwara, Nucl. Phys. **B173**, 487 (1980).

[32]J. R. Cudell et al., Phys. Lett. B **175**, 227 (1986).

[33]R. M. Godbole and D. P. Roy, Z. Phys. C **42**, 219 (1989).

[34]W. H. Smith, in Proceedings of the 11th International Conference on Neutrino Physics and Astrophysics, Dortmund, West Germany, 1984, edited by K. Kleinknecht and E. A. Paschos (World Scientific, Singapore, 1984), p. 442.

[35]D. C. Carey, NUADA-A neutrino flux computer program, June 1975 (unpublished).

[36]A. Malensak and L. Stutte, Fermilab Report No. TM 1990, 1983 (unpublished).

[37]H. Foeth et al., Nucl. Instrum. Methods **A253**, 245 (1987).

[38]Details of this analysis can be found in Vivek Jain, Ph.D. thesis, University of Hawaii, 1988.

[39]A "bunch" is defined to be a group of consecutively hit tubes in a set of two layers. Tubes in one layer are even numbered, and are odd numbered in the adjacent (staggered) layer. For instance, if tubes 72 and 74 are hit in one layer, and 73 and 75 hit in the adjacent layer, then the bunch 72–75 is made for the layer pair.

[40]J. L. Orthel, Ph.D. thesis, Lawrence Berkeley Laboratory, University of California, Report No. LBL-10035, 1979. Since the Monte Carlo program was written for a different experiment, the results had to be corrected for differences in the interaction length (resulting from the different bubble-chamber liquid) and energy spectrum of the tracks.

[41]The kaon fraction is estimated by assuming that the charged-kaon fraction is equal to the corrected neutral-kaon fraction in the charged-current events. The proton fraction is obtained from W. M. Yeagar et al., Phys. Rev. D **16**, 1294 (1977); T. H. Burnett et al., Phys. Lett. **77B**, 443 (1978).

[42]Fermilab-IHEP-ITEP-Michigan Neutrino Group, Phys. Rev. Lett. **39**, 382 (1977).

[43]C. H. Lai, Phys. Rev. D **18**, 1422 (1978).

[44]K. Lang, Ph.D. thesis, University of Rochester, New York, 1985.

[45]The V^0 in 23 271 207 is ambiguous because one of its tracks interacts and thus its momentum is not well measured, whereas the other three ambiguities in Table II are well measured but fit with both Λ and K^0 hypotheses. Therefore, the ambiguities are treated differently. In Ref. 15, eight K^0's and two Λ's were observed in dimuon events. Thus, a probability of 80% is assigned to the V^0 of being a K^0.

[46]C. Peterson et al., Phys. Rev. D 27, 105 (1983).

[47]J. Dorfan, in Proceedings of the 1983 International Symposium on Lepton and Photon Interactions at High Energies, Ithaca, New York, 1983, edited by D. G. Cassel and D. L. Kreinick (Newman Laboratory for Nuclear Studies, Cornell University, Ithaca, 1983).

[48]J. Blietschau et al., Phys. Lett. 86B, 108 (1979).

[49]Particle Data Group, M. Aguilar-Benitez et al., Phys. Lett. 170B, 242 (1986).

[50]C. Foudas, Ph.D. thesis, Columbia University, Nevis Labs, Thesis No. 272, 1989.